IJMSO

International Journal of Mathematical Sciences and Optimization: Theory and Applications
Vol. 9, No. 1, pp. 81 - 103
https://doi.org/10.5281/zenodo.8218016

Entropy optimization and heat transfer analysis of MHD heat generating fluid flow through an anisotropic porous parallel wall channel: An analytic solution

H. A. Isede[1*], A. Adeniyan[2], O.O. Oladosu[3]

1,2,3 Department of Mathematics, University of Lagos, Akoka, Lagos State.
* Corresponding author: hisede@unilag.edu.ng

Article Info
Received: 13 June 2023 Revised: 18 July 2023
Accepted: 22 July 2023 Available online: 30 July 2023

Abstract

This communication carries out an analytic study on entropy optimization and heat spreading of an electrically conducting Newtonian fluid flow within permeable and parallel wall channel in a horizontal orientation. The medium is anisotropic porous passage and permeated by a uniform transverse magnetic field. Internal heat generation and heating friction are considered. Relevance and applications dwell in underground sewage and catalytic transportation as well as in liquid flow rheostats and sensors. Appropriate scaling alterations are administered to convert the governing partial differential equations (PDEs) to ordinary differential equations (ODEs). By means of the Laplace's transform approach the solutions via basic flow controlling parameters values are evaluated exactly. Fluid dimensionless velocity and temperature distributions are sorted out based on the selected figures of embedded parameters, and their impacts examined quantitatively and studied in detail via graphs on heat transfer rate, Bejan number and entropy generation factor. Among others, our findings predict that suction-based viscosity parameter, magnetic and anisotropic permeability parameters retract the dimensionless axial velocity, whereas the entropy generation increases significantly by improved viscous dissipation. Escalation of fluid temperature is predetermined by medium anisotropy. Additionally, further outcomes unveil that not only Peclet and Reynolds based suctions fail to achieve an impact on the entropy generation but also the heat generation at the channel centerline.

Keywords: Channel flow; porous medium; Laplace's transform method; surface heat flux; entropy generation.
MSC2010: 76D99.

IJMSO

International Journal of Mathematical Sciences and Optimization: Theory and Applications
Vol. 9, No. 1, pp. 81 - 103
https://doi.org/10.5281/zenodo.8218016

1 Introduction

The fundamental pioneering knowledge of entropy generation which accounts for the irreversibility of some thermal processes is handsomely based on the second law of thermodynamics. This law reiterates that all processes in practice are inherently irreversible. Entropy generation mechanism remains an important factor used for predicting the minimization of destructive available work/energy for a majority of engineering devices and components such as in heat exchangers, bladed and/or bladeless turbines, gas turbines, energy harvesters and many power-consuming industrial and technical appliances.

Many a researcher has shown keen interest and studied entropy optimization on several body surfaces frequently encountered in system processes initiated by Bejan [1,2]. In his pioneering studies, he has shown that minimizing irreversibility in any thermodynamic system is tantamount to reducing the operating cost and unplanned wastages. It finds applications in refrigeration plants, system upgrading of equipment and production work surveillance, and many more.

Adopting Darcy-Brinkman-Forchheimer model, [3] analyzed numerically via the finite volume method (FVM), the entropy generation of MHD buoyant and forced convection one-phase nanofluid flow through a vertical porous channel subjected to adiabatic wall temperature and medium porous structure. They reported that the entropy generation is promoted generally by increasing the inherent fluid parameters. More recently, [4] presented a new insight regarding reformulation of the two Bejan numbers derived from the first law of thermodynamics. Their analysis unveiled the role and physical meaning of this number as criterion of non-dimensional variable. Enhanced upgrade in thermal systems and energy during heat spreading in fluid convection is of considerable importance to material process engineers and manufacturing developers, amongst others. Beneficial and prevailing applications as itemized above draw the attention of a number of researchers into the ensuing entropy analysis study in thermal systems.

In their maiden investigation into the heat and mass transfer of a conductive Casson fluid flow within an inclined microchannel, [5] established that entropy generation rate decreases at the walls with increasing Hartmann number while noticeable decrements emerge at the center region. Makinde and Azeez [6] conceptualize on second law analysis via a pressure driven steady Newtonian fluid flow through a channel with asymmetric wall convective cooling and variable viscosity. They found that strengthening viscous dissipation can promote the entropy generation rate as well as the dominant structure of the fluid friction irreversibility. More recent report of [7] on hydromagnetic entropy penetration of non-Newtonian micropolar fluid boundary layer flow in the neighborhood of a nonlinearly elongating sheet establishes that viscous and Ohmic dissipation dwindle the Bejan factor.

The problems of convective hydrodynamic fluid flow in anisotropic porous media in both macro- and micro-channels are significantly important; most especially in agro-allied engineering and geologically related applications such as in underground water pollution control, river dam acidification alongside the mine drainage, thermal insulation in buried heat resistant cables, catalytic fixed-bed reactors for biodiesel production, amongst others. [8] have conducted a transient natural convection study of fluid flow in the region interlaced by porous anisotropic permeability between two concentric annular cylinders, and predicted that the effect of temperature stratification further stabilizes and regulates the fluid flow. Using spectral local linearization method (SLLM); [9] have shown that both thermal and solutal stratifications unreservedly influence the boundary-layer viscous hydromagnetic dual convection of a viscoelastic fluid past an inclined permeable cylinder enshrined in Darcy resistant porous medium. A handful of studies on channel flow at variant physical properties have appeared in literature [10–17,36].

The practical importance of heat source or heat generation may arise from a variety of causes such as radioactivity, dissociating fluids, fluid undergoing exothermic or endothermic chemical reactions, release of latent heat due to water vapor condensation; the occurrence of which is very often observable when rain is about to fall in some sub-Sahara regions, etc., the reverse cause of which may constitute heat sink or absorption.

In many convection fluid flows, attributes of body forces cannot be overruled; they play very significant roles as per triggering and/ or controlling the fluid transportation as well as thermal spreading.

IJMSO

International Journal of Mathematical Sciences and Optimization: Theory and Applications
Vol. 9, No. 1, pp. 81 - 103
https://doi.org/10.5281/zenodo.8218016

The influence of Lorentz force (considerably comparable with other hydrodynamic forces), which frequently manifests in an electrically conductive moving fluid traversed by a substantial magnitude of the applied magnetic field, finds its relevant applicability in several system processes of non-mechanical speed-control ensuing in manufacturing and production activities. Considerable applications are encountered in many high-technological devises such as hydromagnetic power generators, high-speed electronics coolants, magneto-aerodynamic ovens, smelt and molten metal purifications, and so forth [18]. The classical unidirectional laminar flow problem of an incompressible and viscous electrically conductive fluid permeated by a non-varying magnetic field; applied transversely to the parallel walls of the channel was pioneered ab initio by [19]. Numerous extensions of this work prevail with ramifications in [20–24] and many other researches. [25] examined the impact of magnetic and electric fields on the convective cooling process of liquid metal flow within a duct. Their findings signified that impressed magnetic or electric field could remarkably enhance or attenuate heat transfer factor. More recently, [26, 37] examined and solved exactly the peristatic flow of a micropolar fluid within an asymmetric channel subject to Lorentz and Darcy forces, heat generation and variable thermal conductivity. They considered the effect of wall slips. Amongst others, their findings stipulate that admittance of the Lorentz force into the flow has the tendency to eliminate bolus formation.
The main theme of the current model is pivoted on examining the effects of anisotropy porous structure on electrically conducting fluid amidst transversely imposed magnetic field vis-à-vis the classical Hartmann flow problem. Reactions of the fluid behaviors consequential to the alterations in viscosity Reynolds and thermal diffusion Peclet numbers as well as dissipative Brinkman are accounted for and discussed in detail aposteriori, constraints encompassed with the entropy generation and Bejan number.

2 Mathematical Formulation

Consider steady, laminar fully developed two-dimensional flow of a viscous and electrically conducting fluid saturated in a simple anisotropic porous medium; bounded by permeable parallel wall of infinite extent in a horizontal geometrical configuration as depicted by Figure 1. The lower and upper walls of the channels are subjected to lateral mass injection and suctions respectively. Both channel walls are directly exposed to uniform thermal flux q, and the flow is pressure-gradient driven. The choice of coordinate system indicates that x-axis is along the centerline, while perpendicular to it is the y-coordinate axis. The applied uniform magnetic induction B_0, is aligned parallel with the y-axis. The axial and transverse velocities are u and v. is the inlet temperature, T is the fluid temperature. Hydrodynamic pressure and fluid density are and respectively. Internal heat generation is Q_0.

$$\nabla \cdot V = 0 \ , \tag{2.1}$$

$$\rho V \cdot \nabla V = -\nabla p + \mu \nabla^2 V + J \wedge B + \frac{\mu}{\overline{\overline{K}}} V \ , \tag{2.2}$$

$$(\rho C_p) V \cdot \nabla T = k \nabla^2 T + \frac{J^2}{\sigma} + Q_0 \left(T + T_0\right) + \mu \phi \ . \tag{2.3}$$

Where electric current density [34, 35] is

$$J = \sigma \left(E + V \wedge B + \frac{1}{Ne} \nabla p_e \right) \ . \tag{2.4}$$

$$\phi = 2 \left[\left(\frac{\partial u}{\partial x} \right)^2 + \left(\frac{\partial v}{\partial y} \right)^2 + \frac{1}{2} \left(\frac{\partial u}{\partial y} + \frac{\partial v}{\partial x} \right)^2 \right] \tag{2.5}$$

IJMSO
International Journal of Mathematical Sciences and Optimization: Theory and Applications
Vol. 9, No. 1, pp. 81 - 103
https://doi.org/10.5281/zenodo.8218016

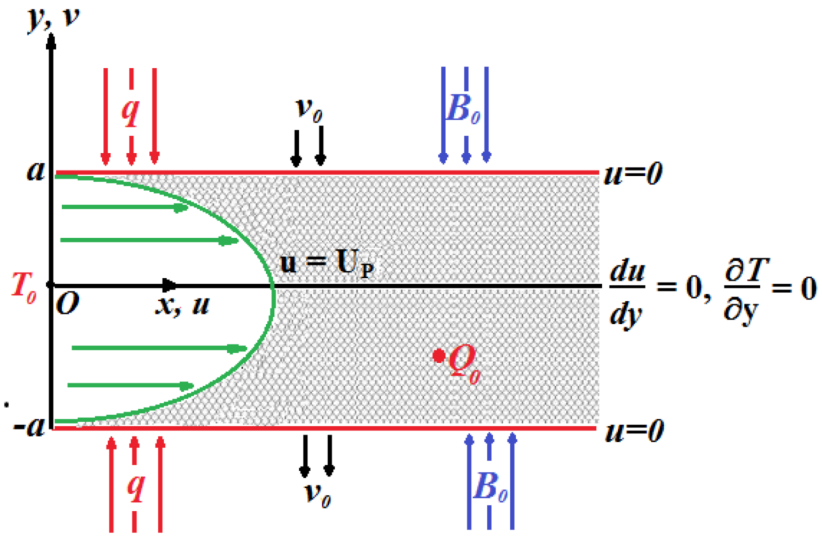

Figure 1: Schematic Diagram of the Physical Model

is the heat dissipation function. Additionally, N, e and p_e are respectively number density, electronic charge and the electron pressure; $\mathbf{E}$, $\mathbf{B}$ are electric and magnetic fields, $\mathbf{V} = (u, v)$, whilst the following usual operators

$$\nabla = \left(\frac{\partial}{\partial x}, \frac{\partial}{\partial y}\right) \ , \ \nabla^2 = \left(\frac{\partial^2}{\partial x^2} + \frac{\partial^2}{\partial y^2}\right) \tag{2.6}$$

In the absence of Hall current and Magnetic Reynolds number $Rm(= \sigma\mu_e a U_0)$, μ_e being the magnetic permeability of the medium, assumptions are made that electron pressure gradient $\nabla p_e = 0$ and $\mathbf{E} = 0$. More so, the symmetrical second-order permeability anisotropic tensor of the fluid-saturated porous medium [27, 28] is

$$\overline{\overline{K}} = \begin{pmatrix} K_1 cos^2\theta + K_2 sin^2\theta & (K_1 - K_2) sin\theta cos\theta \\ (K_1 - K_2) sin\theta cos\theta & K_2 cos^2\theta + K_1 sin^2\theta \end{pmatrix} \ , \tag{2.7}$$

Herein, K_1 and K_2 represent the permeabilities along the principal axes of the porous matrix while the orientation angle between the horizontal and the principal axis with permeability K_2 is θ. The dynamic viscosity is μ. Insertion of (4) - (7) into (1) - (3) gives the component form of conservation equations as

$$\frac{\partial u}{\partial x} + \frac{\partial v}{\partial y} = 0 \ , \tag{2.8}$$

$$a\left(u\frac{\partial u}{\partial x} + v\frac{\partial u}{\partial y}\right) + b\left(u\frac{\partial v}{\partial x} + v\frac{\partial v}{\partial y}\right) = \begin{bmatrix} a\left(-\frac{1}{\rho}\frac{\partial p}{\partial x} + \frac{\mu}{\rho}\nabla^2 u - \frac{\sigma B_0^2}{\rho}u\right) \\ +b\left(-\frac{1}{\rho}\frac{\partial p}{\partial y} + \frac{\mu}{\rho}\nabla^2 v\right) - \frac{\mu}{\rho K_2}u \end{bmatrix} \tag{2.9}$$

$$b\left(u\frac{\partial u}{\partial x} + v\frac{\partial u}{\partial y}\right) + c\left(u\frac{\partial v}{\partial x} + v\frac{\partial v}{\partial y}\right) = \begin{bmatrix} b\left(-\frac{1}{\rho}\frac{\partial p}{\partial x} + \frac{\mu}{\rho}\nabla^2 u - \frac{\sigma B_0^2}{\rho}u\right) \\ +c\left(-\frac{1}{\rho}\frac{\partial p}{\partial y} + \frac{\mu}{\rho}\nabla^2 v\right) - \frac{\mu}{\rho K_2}u \end{bmatrix} \tag{2.10}$$

Where $a = k_1 1$, $b = k_1 2 = k_2 1$, $c = k_2 2$, in (7)

$$\rho C_p\left(u\frac{\partial T}{\partial x} + v\frac{\partial T}{\partial y}\right) = k\left(\frac{\partial^2 T}{\partial x^2} + \frac{\partial^2 T}{\partial y^2}\right) + \sigma B_0^2 u^2 + \mu\left(\frac{u^2}{\kappa_1} + \ fracv^2\kappa_2\right)$$

IJMSO
International Journal of Mathematical Sciences and Optimization: Theory and Applications
Vol. 9, No. 1, pp. 81 - 103
https://doi.org/10.5281/zenodo.8218016

$$+ 2\mu \left[\left(\frac{\partial u}{\partial x} \right)^2 + \left(\frac{\partial v}{\partial y} \right)^2 + \frac{1}{2} \left(\frac{\partial u}{\partial y} + \frac{\partial v}{\partial x} \right)^2 \right] \tag{2.11}$$

Equations (9) - (10) are further simplified and rearranged to obtain

$$u\frac{\partial u}{\partial x} + v\frac{\partial u}{\partial y} = -\frac{1}{\rho}\frac{\partial p}{\partial x} + \frac{\mu}{\rho}\nabla^2 u - \frac{\sigma B_0^2}{\rho}u - \frac{\mu}{\rho K_2}cu \quad , \tag{2.12}$$

Where $\mathbf{c} = cos^2\theta + K^* sin^2\theta$, a special case for which $\theta = \pi/2$, as in (12) signifies $\mathbf{c}$ as the anisotropy parameter, whereas $K^* = K_1/K_2$ is the ratio of permeabilities.

Boundary conditions:

$$\left.\begin{array}{l} u(x,-a) = 0,\ v(x,-a) = v_0\ ,\ \left.\frac{\partial T}{\partial y}\right|_{(x,-a)} = -\frac{q}{k}\ , \\ u(x,0) = U_p,\ \left.\frac{\partial u}{\partial y}\right|_{(x,0)} = 0\ ,\ T(0,0) = T_0\ ,\ \left.\frac{\partial T}{\partial y}\right|_{(x,0)} = 0\ , \\ u(x,a) = 0,\ v(x,a) = v_0,\ \left.\frac{\partial T}{\partial y}\right|_{(x,a)} = -\frac{q}{k}\ . \end{array}\right\} \tag{2.13}$$

Where U_p, q, k and C_p are peak velocity at channel centerline, wall heat flux, thermal conductivity and specific heat of the fluid respectively. It is worthy to mention that of the stated boundary conditions, two of them are indeed essential for solving (9) - (12). This simulation presumes that the uniform lateral mass flux, $v = -v_0$. Thusly, (8) reveals that

$$v = -v_0\ , u = u(y)\ , -\infty < -a \le y \le a < \infty\ , x \ge 0. \tag{2.14}$$

Presenting the under-listed scaling variables:

$$\left.\begin{array}{l} X = \frac{\alpha x}{v_0 a^2},\ Y = \frac{y}{a}\ ,\ U = \frac{u}{U_0}\ ,\ P = \frac{q}{\rho U_0^2 Pr}\ , \\ Ha = B_0 a\sqrt{\frac{\sigma}{\mu}},\ Da^{-1} = \frac{K_2}{a^2}\ ,\ \Theta = \frac{k(T-T_0)}{qa}\ ,\ Re = \frac{av_0}{\nu}\ , \end{array}\right\} \tag{2.15}$$

and using them via (14) in (9) - (12) to obtain the following ODEs alongside; the accompanied boundary conditions in cognizance of symmetry about the dimensionless centerline, and neglecting channel end-effects:

$$\frac{d^2U}{dY^2} + Re\frac{dU}{dY} - \left(Ha^2 + cDa^{-1}\right)U = -G \tag{2.16}$$

$$\frac{\partial^2\Theta}{\partial Y^2} + Pe\frac{\partial\Theta}{\partial Y} + Q\Theta = \lambda U - Br\left[\left(Ha^2 + Da^{-1}\right)U^2 + \left(\frac{dU}{dY}\right)^2\right]\ , \tag{2.17}$$

Herein, U_0 denotes scaled velocity, $\nu = \left(\frac{\nu}{\rho}\right)$ is the kinematic viscosity, $Re\left(=\frac{a\nu_0}{\nu}\right)$ is suction-based Reynolds number, $\varepsilon\left(=\frac{U_p}{U_0}\right)$ is the velocity ratio, $\alpha\left(=\frac{k}{\rho C_p}\right)$ is the thermal diffusion coefficient, Ha and Da^{-1}, are respectively Hartmann and inverse Darcy numbers, $Pr\left(=\frac{\nu}{\alpha}\right)$, $Br\left(=\frac{\nu U_0^2}{qa}\right)$ and $Pe\left(=\frac{a\nu_0}{\alpha}\right)$ are Prandtl, Brinkman and suction-based Peclet numbers respectively. The dimensionless constant axial adverse temperature gradient $\lambda\left(=\frac{\partial\Theta}{\partial X}\right)$, [29, 30]. Nonetheless, if the wall temperature is constant and the flow is thermally and hydrodynamically fully developed then $\lambda = 0$ [26]. Also $Q\left(=\frac{Q_0 a^2}{k}\right)$ is heat generation/absorption parameter, $G\left(=-\frac{dP}{dX}\right)$ is the dimensionless pressure gradient. By replacing injection wall velocity $\nu = -\nu_0$ with suction $\nu = \nu_0$ in our present non-dimensional equations of momentum and energy; neglecting permeability of the porous medium and heat generation/absorption, successfully we recover those of [31]. Furthermore, $Pe = 0$ signifies that the flow is purely diffusive heat transfer. Letting

$$Re = A\ , G = -C\ , Ha^2 + cDa^{-1} = B\ , \tag{2.18}$$

IJMSO
International Journal of Mathematical Sciences and Optimization: Theory and Applications
Vol. 9, No. 1, pp. 81 - 103
https://doi.org/10.5281/zenodo.8218016

whereas the Laplace Transform (LT) of U, being

$$\bar{U}(S) = \int_0^\infty exp(-SY)U(Y)dY \ , \tag{2.19}$$

and $S > 0$, is the Laplace transform parameter. Now taking LT of (16) after mere rearrangement of terms and simplification, to have

$$\bar{U} = \frac{\varepsilon S^2 + \varepsilon AS + C}{S(S^2 + AS - B)} \tag{2.20}$$

One now resolves (20) into partial fractions and write

$$\bar{U} = \frac{D_1}{S} + \frac{D_2}{2S + A + \sqrt{(A^2 + 4B)}} + \frac{D_3}{2S + A - \sqrt{(A^2 + 4B)}} \tag{2.21}$$

Whereby D_1, D_2, D_3 are to be determined. Imposing the solvability conditions on (21) in terms of Laplace variable S, solving the three encompassed obtained equations simultaneously,

$$\begin{gathered} D_1 = -\tfrac{C}{B} \ , \quad D_2 = \tfrac{(Be+C)(\sqrt{(A^2+4B)}-A)}{B\sqrt{(A^2+4B)}} \ , \\ D_3 = \tfrac{(B\varepsilon+C)(\sqrt{(A^2+4B)}+A)}{B\sqrt{(A^2+4B)}} \ , \end{gathered} \tag{2.22}$$

Nonetheless, taking the inverse LT of (21), substituting (22), we find

$$\left.\begin{aligned} &U(Y) = D_1 + \tfrac{D_2}{2} exp\left(\tfrac{A+\sqrt{(A^2+4B)}}{2}Y\right) + \tfrac{D_3}{2} exp\left(\tfrac{A-\sqrt{(A^2+4B)}}{2}Y\right) \\ &Or\ its\ replicate \\ &U = D_1 + \tfrac{1}{2}exp\left(-\tfrac{A}{2}Y\right)\left[(D_3 + D_2)coshY\sqrt{A^2 + 4B}\right. \\ &\qquad\qquad \left. + (D_3 - D_2)sinhY\sqrt{A^2 + 4B}\ \right] \end{aligned}\right\} \tag{2.23}$$

Succinct scrutiny of (17) reveals that the equation is indeed a mixture of PDE and ODE, and in consequence one needs to invoke the LT with respect to coordinate variable X. This may be expressed as

$$\bar{\Theta}(S, Y) = \int_0^\infty exp(-SX)\Theta(X, Y)dX \ . \tag{2.24}$$

Worthy to reiterate, is the prudent assumption of constancy of the dimensionless adverse temperature gradient $\lambda = \frac{\partial \Theta}{\partial X}$ which integrates to yield

$$\Theta = \lambda X + F(Y) \ , \tag{2.25}$$

wherein X and $F(Y)$ are correspondingly the dimensionless axial position and arbitrary function of Y.
Applying LT on (17) after substituting (25), one obtains

$$\frac{d^2\bar{\Theta}}{dY^2} + \beta\frac{d\bar{\Theta}}{dY} + Q\bar{\Theta} = \frac{1}{S}\left\{\lambda U - \left[\gamma U^2 + Br\left(\frac{dU}{dY}\right)^2\right]\right\} \tag{2.26}$$

Where

$$\beta = Pe \ , \ \gamma = Br\left(Ha + Da^{-1}\right) \ . \tag{2.27}$$

IJMSO

International Journal of Mathematical Sciences and Optimization: Theory and Applications
Vol. 9, No. 1, pp. 81 - 103
https://doi.org/10.5281/zenodo.8218016

Evaluating the homogeneous part of (26), the resulting complementary primitive function is

$$\bar{\Theta}_c = E_1 e^{\frac{-\beta+\sqrt{\beta^2-4S_H}}{2}Y} + E_2 e^{\frac{-\beta-\sqrt{\beta^2-4S_H}}{2}Y}\ , \tag{2.28}$$

Where E_1 and E_2 are integration arbitrary constants. The particular integral of (26) via (28) proffers

$$\bar{\Theta}_p = \frac{1}{S}\left(\begin{array}{l} \frac{(\lambda-\gamma D_1)D_1}{Q} + \frac{\left(\frac{\alpha}{2}-\gamma D_1\right)D_2 e^{-\left(\frac{A+\sqrt{(A^2+4B)}}{2}\right)Y}}{\left(\frac{A+\sqrt{(A^2+4B)}}{2}\right)^2-\beta\left(\frac{A+\sqrt{(A^2+4B)}}{2}\right)+Q} \\ + \frac{\left(\frac{\alpha}{2}-\gamma D_1\right)D_3 e^{-\left(\frac{A-\sqrt{(A^2+4B)}}{2}\right)Y}}{\left(\frac{A-\sqrt{(A^2+4B)}}{2}\right)^2-\beta\left(\frac{A-\sqrt{(A^2+4B)}}{2}\right)+Q} \\ - \frac{\left(\gamma+Br\frac{\left(A+\sqrt{(A^2+4B)}\right)^2}{4}\right)\frac{D_2^2}{4}e^{-\left(A+\sqrt{(A^2+4B)}\right)Y}}{\left(A+\sqrt{(A^2+4B)}\right)^2-\beta\left(A+\sqrt{(A^2+4B)}\right)+Q} \\ - \frac{\left(\gamma+Br\frac{\left(A-\sqrt{(A^2+4B)}\right)^2}{4}\right)\frac{D_3^2}{4}e^{-\left(A-\sqrt{(A^2+4B)}\right)Y}}{\left(A-\sqrt{(A^2+4B)}\right)^2-\beta\left(A-\sqrt{(A^2+4B)}\right)+Q} \\ - \frac{(\gamma-BrB)\frac{D_2D_3}{2}e^{-AY}}{A^2-\beta A+Q} \end{array}\right) \tag{2.29}$$

Thusly, the general solution of obtained ODE (26) reads as $\bar{\Theta} = \bar{\Theta}_c + \bar{\Theta}_p$, is inverted Laplacianly in terms of S to give

$$\Theta(X,Y) = \lambda X + \left(\begin{array}{l} \left(E_1 e^{-\left(\frac{\beta-\sqrt{\beta^2-4S_H}}{2}\right)Y} + E_2 e^{-\left(\frac{\beta+\sqrt{\beta^2-4S_H}}{2}\right)Y}\right)\delta(X) \\ - \frac{(\gamma-BrB)\frac{D_2D_3}{2}e^{-AY}}{A^2-\beta A+Q} + \frac{\left(\frac{\alpha}{2}-\gamma D_1\right)D_2 e^{-\left(\frac{A+\sqrt{(A^2+4B)}}{2}\right)Y}}{\left(\frac{A+\sqrt{(A^2+4B)}}{2}\right)^2-\beta\left(\frac{A+\sqrt{(A^2+4B)}}{2}\right)+Q} \\ + \frac{(\lambda-\gamma D_1)D_1}{Q} + \frac{\left(\frac{\alpha}{2}-\gamma D_1\right)D_3 e^{-\left(\frac{A-\sqrt{(A^2+4B)}}{2}\right)Y}}{\left(\frac{A-\sqrt{(A^2+4B)}}{2}\right)^2-\beta\left(\frac{A-\sqrt{(A^2+4B)}}{2}\right)+Q} \\ - \frac{\left(\gamma+Br\frac{\left(A+\sqrt{(A^2+4B)}\right)^2}{4}\right)\frac{D_2^2}{4}e^{-\left(A+\sqrt{(A^2+4B)}\right)Y}}{\left(A+\sqrt{(A^2+4B)}\right)^2-\beta\left(A+\sqrt{(A^2+4B)}\right)+Q} \\ - \frac{\left(\gamma+Br\frac{\left(A-\sqrt{(A^2+4B)}\right)^2}{4}\right)\frac{D_3^2}{4}e^{-\left(A-\sqrt{(A^2+4B)}\right)Y}}{\left(A-\sqrt{(A^2+4B)}\right)^2-\beta\left(A-\sqrt{(A^2+4B)}\right)+Q} \end{array}\right) \tag{2.30}$$

Herein

$$\delta(X) = \left\{\begin{array}{l} 0\ , X \neq 0 \\ \infty\ , X = 0 \end{array}\right.$$

IJMSO

International Journal of Mathematical Sciences and Optimization: Theory and Applications
Vol. 9, No. 1, pp. 81 - 103
https://doi.org/10.5281/zenodo.8218016

is the so-called Dirac delta, while its inverse Laplace transform is 1. Choosing, among others, the boundary conditions $\frac{\partial\Theta}{\partial Y}(X,0)=0$, $\frac{\partial\Theta}{\partial Y}(X,-1)=-1$, utilizing (30), we find

$$E_1=\begin{pmatrix} e^{\left(\frac{\beta+\sqrt{\beta^2-4Q}}{2}\right)}(F_1+F_2-F_3-F_4-F_5)+1-F_1e^{\left(\frac{A+\sqrt{(A^2+4B)}}{2}\right)} \\ -F_2e^{\left(\frac{A-\sqrt{(A^2+4B)}}{2}\right)}+F_3e^{\left(\frac{A+\sqrt{(A^2+4B)}}{2}\right)}+F_4e^{\left(\frac{A-\sqrt{(A^2+4B)}}{2}\right)}+F_5e^{A} \end{pmatrix}$$
$$+\left[\left(e^{\left(\frac{\beta-\sqrt{(\beta^2-4Q)}}{2}\right)}-e^{\left(\frac{\beta+\sqrt{(\beta^2-4Q)}}{2}\right)}\right)\left(\beta-\sqrt{\beta^2-4Q}\right)\right]^{-1}\frac{2}{\delta(X)} \tag{2.31}$$

$$E_2=\begin{pmatrix} e^{\left(\frac{\beta-\sqrt{\beta^2-4Q}}{2}\right)}(F_1+F_2-F_3-F_4-F_5)+1-F_1e^{\left(\frac{A+\sqrt{(A^2+4B)}}{2}\right)} \\ -F_2e^{\left(\frac{A-\sqrt{(A^2+4B)}}{2}\right)}+F_3e^{\left(\frac{A+\sqrt{(A^2+4B)}}{2}\right)}+F_4e^{\left(\frac{A-\sqrt{(A^2+4B)}}{2}\right)}+F_5e^{A} \end{pmatrix}$$
$$+\left[\left(e^{\left(\frac{\beta+\sqrt{(\beta^2-4Q)}}{2}\right)}-e^{\left(\frac{\beta-\sqrt{(\beta^2-4Q)}}{2}\right)}\right)\left(\beta+\sqrt{\beta^2-4Q}\right)\right]^{-1}\frac{2}{\delta(X)} \tag{2.32}$$

Where

$$F_1=\frac{\left(\frac{\alpha}{2}-\gamma D_1\right)D_2\left(\frac{A+\sqrt{(A^2+4B)}}{2}\right)}{\left(\frac{A+\sqrt{(A^2+4B)}}{2}\right)^2-\beta\left(\frac{A+\sqrt{(A^2+4B)}}{2}\right)+Q}, \tag{2.33}$$

$$F_2=\frac{\left(\frac{\alpha}{2}-\gamma D_1\right)D_3\left(\frac{A-\sqrt{(A^2+4B)}}{2}\right)}{\left(\frac{A-\sqrt{(A^2+4B)}}{2}\right)^2-\beta\left(\frac{A-\sqrt{(A^2+4B)}}{2}\right)+Q}, \tag{2.34}$$

$$F_3=\frac{\left(\gamma+Br\frac{\left(A+\sqrt{(A^2+4B)}\right)^2}{4}\right)\frac{D_2^2}{4}\left(A+\sqrt{(A^2+4B)}\right)}{\left(A+\sqrt{(A^2+4B)}\right)^2-\beta\left(A+\sqrt{(A^2+4B)}\right)+Q}, \tag{2.35}$$

$$F_4=\frac{\left(\gamma+Br\frac{\left(A-\sqrt{(A^2+4B)}\right)^2}{4}\right)\frac{D_3^2}{4}\left(A-\sqrt{(A^2+4B)}\right)}{\left(A-\sqrt{(A^2+4B)}\right)^2-\beta\left(A-\sqrt{(A^2+4B)}\right)+Q}, \tag{2.36}$$

$$F_5=\frac{(\gamma-BrB)\frac{D_2D_3}{2}A}{A^2-\beta A+Q}. \tag{2.37}$$

IJMSO

International Journal of Mathematical Sciences and Optimization: Theory and Applications
Vol. 9, No. 1, pp. 81 - 103
https://doi.org/10.5281/zenodo.8218016

Finally, we find the temperature distribution function as

$$\Theta(X,Y) = \lambda X + \left(\begin{array}{l} (F_1+F_2-F_3-F_4-F_5)\, e^{\frac{\beta}{2}} \left(\frac{e^{\frac{-\sqrt{\beta^2-4S_H}}{2}(1+Y)}}{\beta+\sqrt{\beta^2-4S_H}} \right. \\ \left. - \frac{e^{\frac{\sqrt{\beta^2-4S_H}}{2}(1+Y)}}{\beta-\sqrt{\beta^2-4S_H}} \right) + \left(1 - \left(F_1 e^{\left(\frac{\sqrt{(A^2+4B)}}{2}\right)} \right. \right. \\ \left. \left. + F_2 e^{\left(\frac{-\sqrt{(A^2+4B)}}{2}\right)} \right) e^{\left(\frac{A}{2}\right)} + \left(F_3 e^{\left(\sqrt{(A^2+4B)}\right)} \right. \right. \\ \left. \left. + F_4 e^{\left(-\sqrt{(A^2+4B)}\right)} + F_5 \right) e^{A} \right) \\ \left(\frac{e^{\frac{-\sqrt{\beta^2-4S_H}}{2}Y}}{\beta+\sqrt{\beta^2-4S_H}} - \frac{e^{\frac{\sqrt{\beta^2-4S_H}}{2}Y}}{\beta-\sqrt{\beta^2-4S_H}} \right) \end{array} \right)$$

$$\left(\frac{e^{\frac{-\beta}{2}(1+Y)}}{sinh\left(\frac{\sqrt{\beta^2-4S_H}}{2}\right)} \right) + \left(\frac{F_1 e^{\frac{-\sqrt{(A^2+4B)}}{2}Y}}{A+\sqrt{(A^2+4B)}} + \frac{F_2 e^{\frac{\sqrt{(A^2+4B)}}{2}Y}}{A-\sqrt{(A^2+4B)}} \right) 2e^{\frac{-A}{2}Y}$$

$$- \left(\frac{F_3 e^{-\sqrt{(A^2+4B)}Y}}{A+\sqrt{(A^2+4B)}} + \frac{F_4 e^{\sqrt{(A^2+4B)}Y}}{A-\sqrt{(A^2+4B)}} + \frac{F_5}{A} \right) e^{-AY} + \frac{(\lambda-\gamma D_1)\, D_1}{S_H} \tag{2.38}$$

3 Entropy production and irreversibility process analysis

In accordance with [2], the volumetric rate of local entropy generation in convective heat transfer of an incompressible Newtonian fluid preserving Fourier thermal conduction law may be advanced as [3]

$$S_G = \frac{k}{T_0^2}\left(\left(\frac{\partial T}{\partial x}\right)^2 + \left(\frac{\partial T}{\partial y}\right)^2 \right) + \frac{\mu}{T_0}\left\{ 2\left(\left(\frac{\partial u}{\partial x}\right)^2 + \left(\frac{\partial v}{\partial y}\right)^2 \right) + \left(\frac{\partial u}{\partial y}+\frac{\partial v}{\partial x}\right)^2 \right\}$$
$$+ \frac{1}{T_0}\left(\sigma B_0^2 + \frac{\mu}{\kappa_1}\right)\left(u^2+v^2\right) , \tag{3.1}$$

in which the first term is the local heat dissipated due to thermal conduction, the second term is local viscous heat dissipation, the third term is the local heat dissipation consequential to the Lorentz and Darcy forces. Engineering irreversibility quantity of importance is the Bejan factor (Be). It is usually considered as the ratio of the first term of (39) to the resultant entropy generation [7,32,33]. Thusly,

$$Be = \frac{S_{G,H}}{S_G} , \tag{3.2}$$

where $S_{G,H}$ is the heat generation due to conduction heat transfer, i.e. heat transfer irreversibility. The non-dimensional forms of (39) and (40) alter to

$$N_S = \frac{1}{Pe^2}\left(\frac{\partial \Theta}{\partial X}\right)^2 + \left(\frac{\partial \Theta}{\partial Y}\right)^2 + \frac{Br}{\Omega}\left(\frac{\partial U}{\partial Y}\right)^2 + \left(Ha^2 + \frac{c}{Da}\right)\frac{Br}{\Omega}U^2 , \tag{3.3}$$

IJMSO

International Journal of Mathematical Sciences and Optimization: Theory and Applications
Vol. 9, No. 1, pp. 81 - 103
https://doi.org/10.5281/zenodo.8218016

wherein $N_{C,XY} = N_{CX} + N_{CY} = \frac{1}{Pe^2}\left(\frac{\partial\Theta}{\partial X}\right)^2 + \left(\frac{\partial\Theta}{\partial Y}\right)^2$ and $\Omega = \frac{\Delta T}{T_0}$ denotes the ratio of temperature difference to inlet temperature, i.e. temperature ratio, while the combination of the last two terms is friction irreversibility. Bejan number, may now be expressed as

$$Be = \frac{N_{C,XY}}{N_S} \ , \tag{3.4}$$

in which $0 \leq Be \leq 1$. Heat transfer irreversibility dominance signifies $Be = 1$, and $Be = 0$ depicts predominance of the fluid friction irreversibility. Computations are then carried out and post-processed for various values of the axial and transverse dimensionless temperature, axial non-dimensional velocity and the velocity gradient across the fluid flow within the channel based on carefully selected basic flow parameters.

4 Results and Discussion

A parametric analytical study is carried out comprehensively and scrutinized via plotted graphs. This is done for selected values of flow-control dimensionless materials, viz., heat transfer rate, Bejan number, entropy generation factor, viscosity parameter, magnetic permeability parameter, anisotropic permeability parameter, Darcy, Peclet-based suction, Reynolds-based suctions and heat generation.

The effect of these parameters on the velocity, temperature and entropy generation are analyzed using Maple software and the graphical results are presented as follows.

The impacts due to the variation of major physical parameters, such as the Reynold number (Re), inverse Darcy number (Da^{-1}), the Hartmann number (Ha), the anisotropic parameter (c), and pressure gradient (G), on the velocity profile, are depicted in Figures 2-4, 15, and 20 respectively. It is seen that while increases in Re diminish the velocity profile, increases in Da^{-1}, Ha, c, and G enhances the velocity profile.

The influence of various flow controlling parameters on temperature profiles is demonstrated in Figures 5-8, 16-19, and 21. It is observed in Figure 8 that increase in Da^{-1} shrinks the temperature profile. But increases in the other parameters such as Re, Ha, S_H, G, Br, Pe, c, and X, magnify the temperature profiles.

The response trend of entropy generation rate when the heat generation parameter SH is adjusted is depicted in Figures 9-14. It is seen in Figures 9 and 11 that increases in Pe and Ω reduces the entropy generation profile. While in Figures 10, 12-14 the entropy generation profile is boosted with increases in Br, Re, Da^{-1}, and S_H.

IJMSO
International Journal of Mathematical Sciences and Optimization: Theory and Applications
Vol. 9, No. 1, pp. 81 - 103
https://doi.org/10.5281/zenodo.8218016

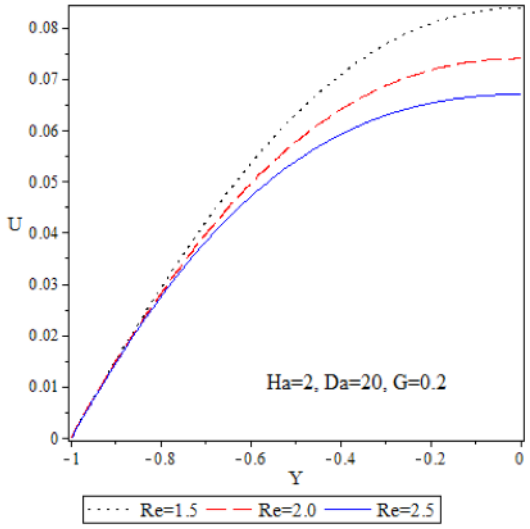

Figure 2: Velocity profile decrease as Reynold number (Re) increases.

5 Concluding remarks

This is an analytic study on entropy optimization and heat spreading of an electrically conducting Newtonian fluid flow within a permeable and parallel wall channel on a horizontal orientation. The medium is an anisotropic porous passage, permeated by a uniform transverse magnetic field. The Internal heat generation and heating friction are considered.
The scaled governing equations are solved by means of the Laplace's transform approach, and the solutions, via basic flow controlling parameters values are evaluated exactly.
Analyses of the impact of the fluid dimensionless velocity and temperature are examined quantitatively and studied in detail via graphs on heat transfer rate, Bejan number and entropy generation factor.
Among others, the important findings predict that suction-based viscosity parameter, magnetic and anisotropic permeability parameters retract the dimensionless axial velocity, whereas the entropy generation increases significantly by improved viscous dissipation. The upsurge of fluid temperature is predetermined by medium anisotropy. Also, it is not only the Peclet and Reynolds based suctions that fail to achieve an impact on the entropy generation, [38] Casson-Williamson flow, stretching plate, 2-phase nanofluid, slips, generation at the channel centerline.

References

[1] A. Bejan, A study of entropy generation in fundamental convective heat transfer, J. Heat Transfer, 101, 718-725, 1979.

[2] A. Bejan, Second-law analysis in heat transfer and thermal design, Adv. Heat Trans., 15, 1–58, 1982.

[3] I. Fersadou, H. Kahalerras and M. El Ganaoui, MHD mixed convection and entropy generation of a nanofluid in a vertical porous channel, Computers & Fluids, 121, 164-179, 2015.

[4] V. D. Zimparov, M. S. Angelov, J. Y. Hristov, New insight into the definitions of the Bejan number, Int. Commun. Heat Mass Transfer, 116(2020), 104637, 2020.

IJMSO

International Journal of Mathematical Sciences and Optimization: Theory and Applications
Vol. 9, No. 1, pp. 81 - 103
https://doi.org/10.5281/zenodo.8218016

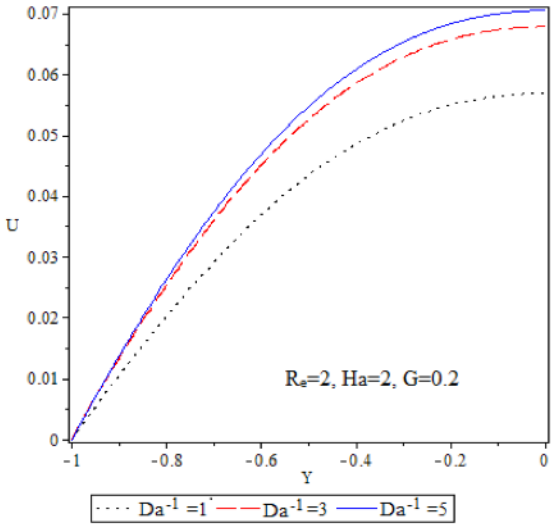

Figure 3: Velocity profile increase as inverse Darcy number (Da^{-1}) increases.

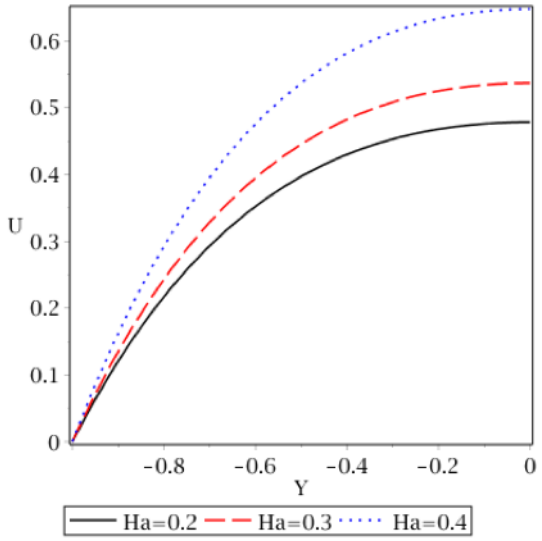

Figure 4: Velocity profile increases as the Hartmann number (Ha) increases.

IJMSO

International Journal of Mathematical Sciences and Optimization: Theory and Applications
Vol. 9, No. 1, pp. 81 - 103
https://doi.org/10.5281/zenodo.8218016

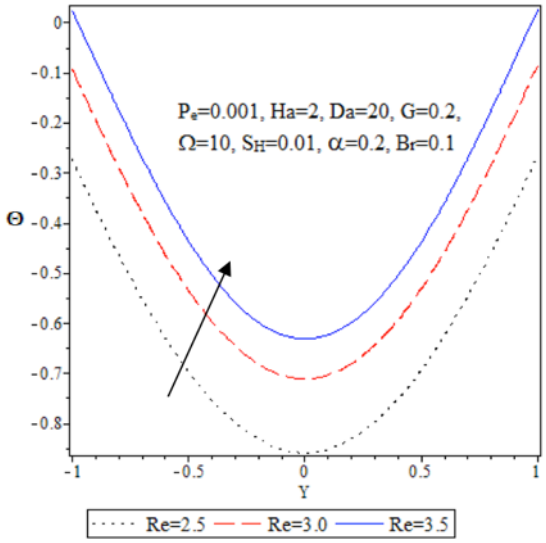

Figure 5: Temperature profile increases as Reynold number (Re) increases.

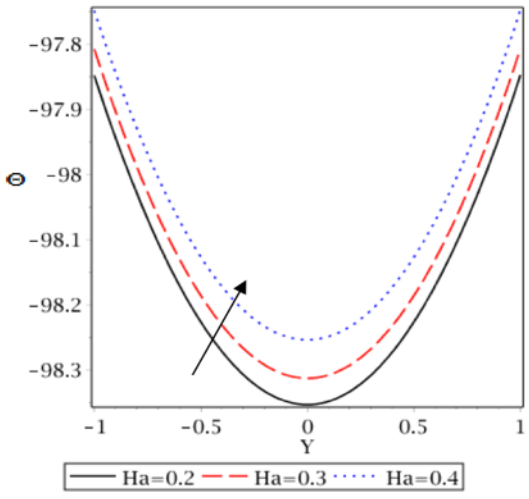

Figure 6: Temperature profile increases as Hartmann number (Ha) increases.

IJMSO

International Journal of Mathematical Sciences and Optimization: Theory and Applications
Vol. 9, No. 1, pp. 81 - 103
https://doi.org/10.5281/zenodo.8218016

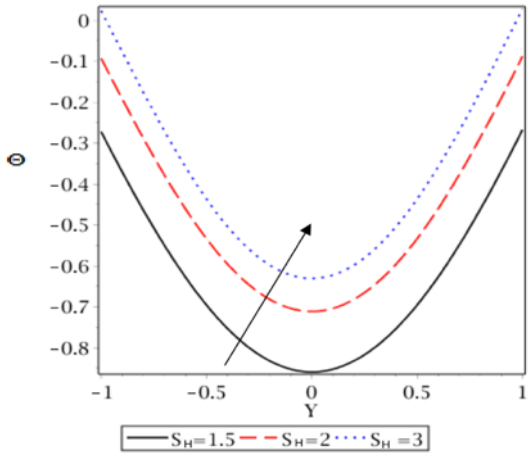

Figure 7: Temperature profile increases as (S_H) increases.

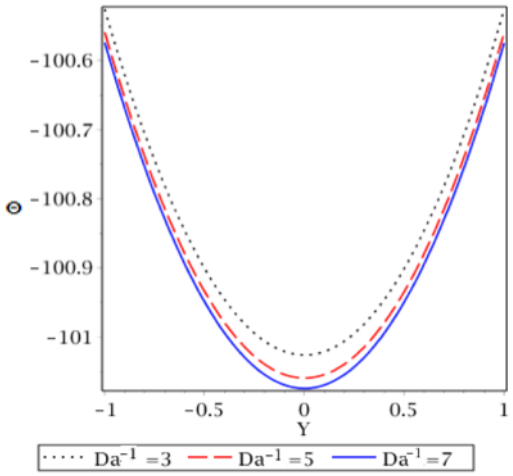

Figure 8: Temperature profile decreases as the inverse Darcy number (Da^{-1}) increases.

IJMSO
International Journal of Mathematical Sciences and Optimization: Theory and Applications
Vol. 9, No. 1, pp. 81 - 103
https://doi.org/10.5281/zenodo.8218016

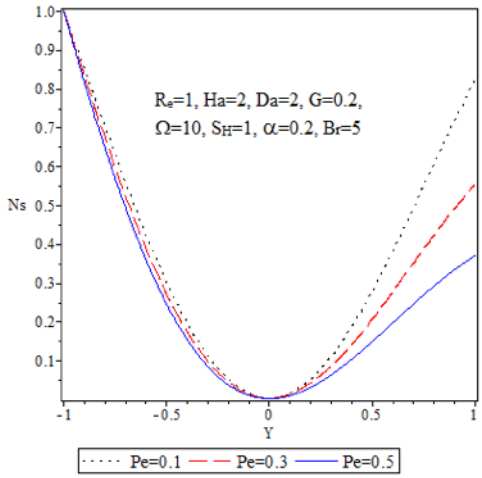

Figure 9: Entropy generation number, N_S profile decreases as Peclet number (Pe) increases.

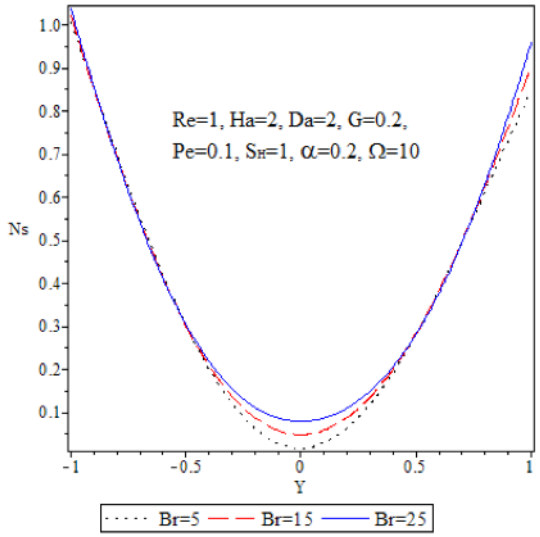

Figure 10: Entropy generation number, N_S profile increases as the Brickman number (Br) increases.

IJMSO
International Journal of Mathematical Sciences and Optimization: Theory and Applications
Vol. 9, No. 1, pp. 81 - 103
https://doi.org/10.5281/zenodo.8218016

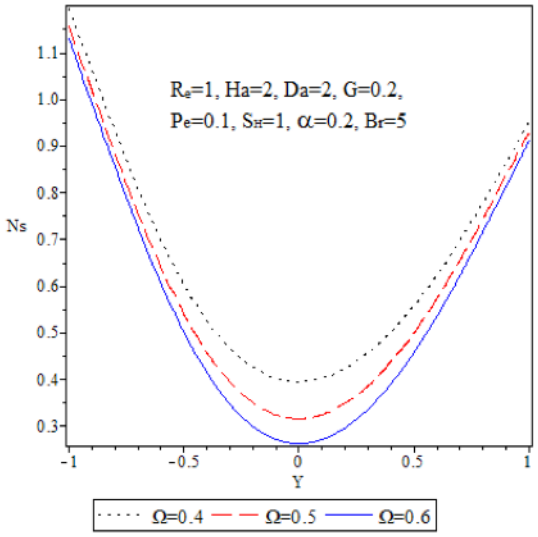

Figure 11: Entropy generation number, N_S profile decreases as Ω increases.

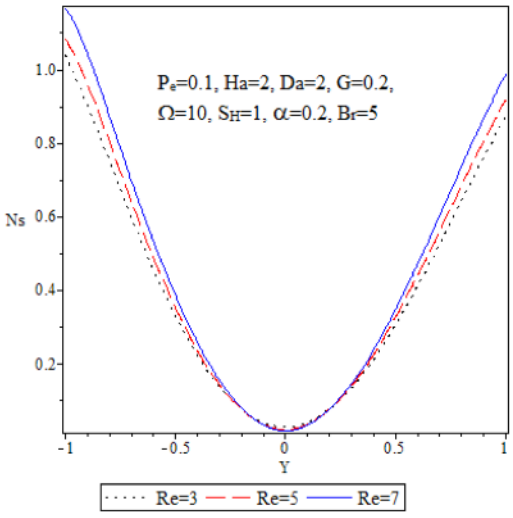

Figure 12: Entropy generation number, N_S profile increases as Reynold number (Re) increases.

IJMSO

International Journal of Mathematical Sciences and Optimization: Theory and Applications
Vol. 9, No. 1, pp. 81 - 103
https://doi.org/10.5281/zenodo.8218016

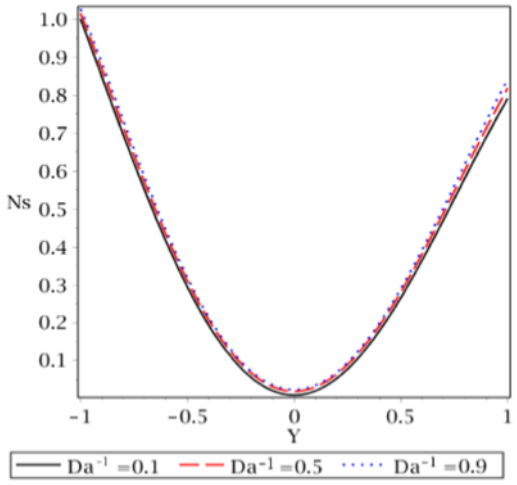

Figure 13: Entropy generation number, N_S profile increases as the inverse Darcy number (Da^{-1}) increases.

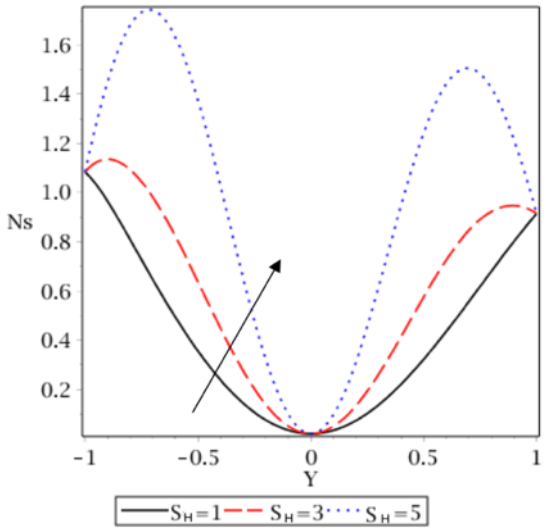

Figure 14: Entropy generation number, N_S profile increases as the heat generation parameter (S_H) increases.

IJMSO
International Journal of Mathematical Sciences and Optimization: Theory and Applications
Vol. 9, No. 1, pp. 81 - 103
https://doi.org/10.5281/zenodo.8218016

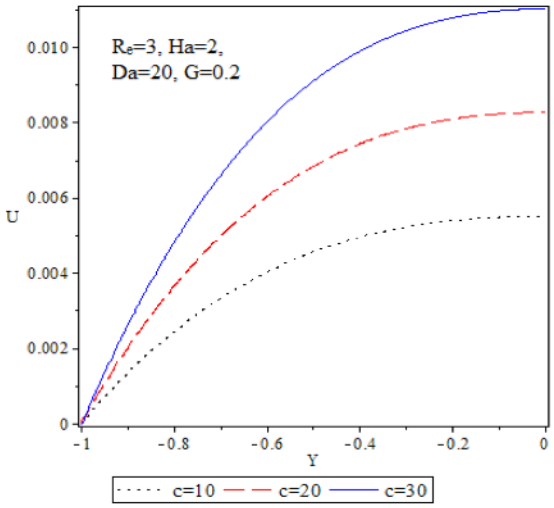

Figure 15: Velocity profile increases as the anisotropy parameter (c) increases.

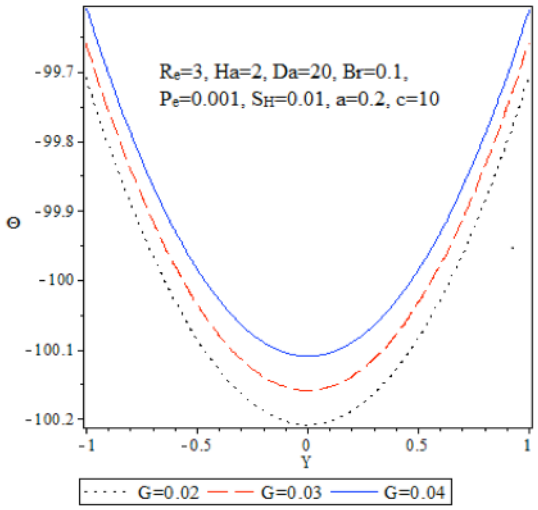

Figure 16: Temperature profiles increases as the pressure gradient G increases.

IJMSO
International Journal of Mathematical Sciences and Optimization: Theory and Applications
Vol. 9, No. 1, pp. 81 - 103
https://doi.org/10.5281/zenodo.8218016

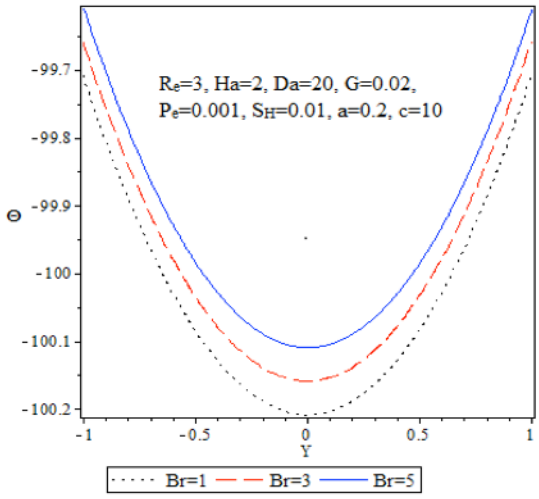

Figure 17: Temperature profiles increases as the Brickman number (Br) increases.

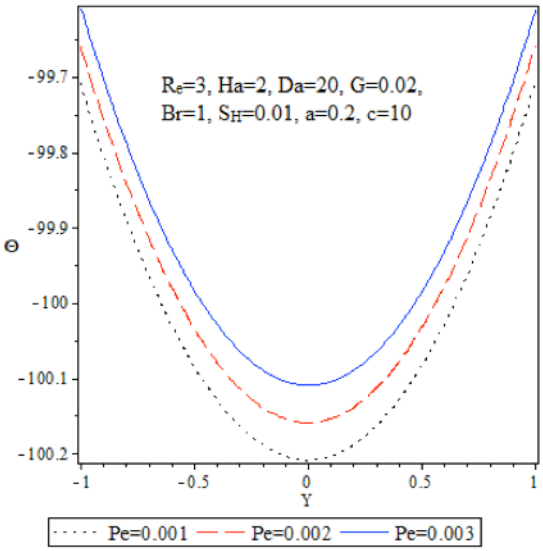

Figure 18: Temperature profiles increases as the Peclet number (Pe) increases.

IJMSO
International Journal of Mathematical Sciences and Optimization: Theory and Applications
Vol. 9, No. 1, pp. 81 - 103
https://doi.org/10.5281/zenodo.8218016

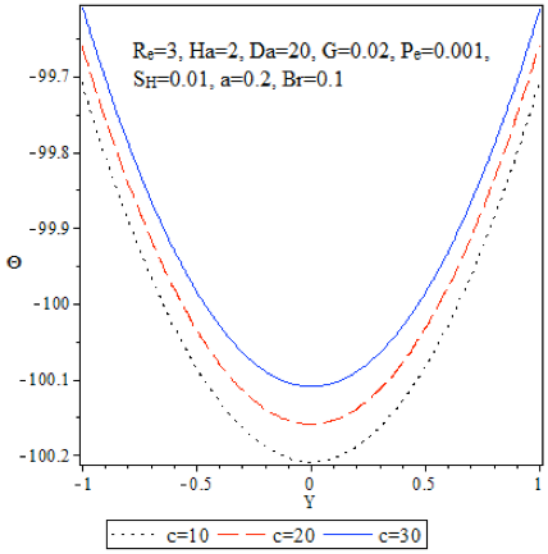

Figure 19: Temperature profiles increases as the anisotropy parameter (c) increases.

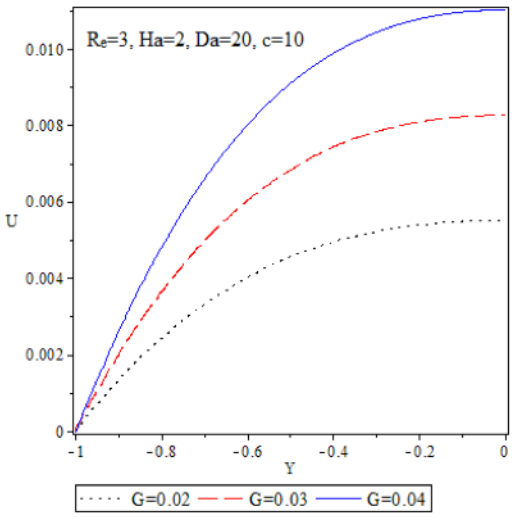

Figure 20: Velocity profiles increases as the pressure gradient (G) is enhanced.

IJMSO
International Journal of Mathematical Sciences and Optimization: Theory and Applications
Vol. 9, No. 1, pp. 81 - 103
https://doi.org/10.5281/zenodo.8218016

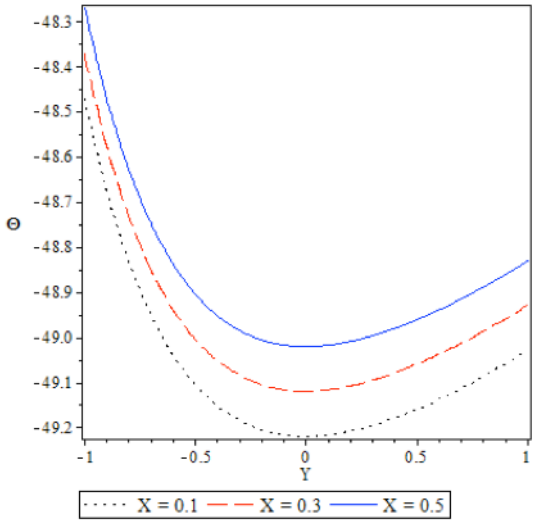

Figure 21: Temperature profiles increases as the axial distance (X) increase.

[5] B. Gireesha, C. T. Srinivasa, N. S. Shashikumar, M. Madhu, J. Singh and B. Mahanthesh, Entropy generation and heat transport analysis of Casson fluid flow with viscous and Joule heating in an inclined porous microchannel, ARCHIVE Proceedings of the Institution of Mechanical Engineers Part E Journal of Process Mechanical Engineering 1989-1996, 10.1177/0954408919849987, 2019.

[6] O. D. Makinde and A. Azeez, Second law analysis for a variable viscosity plane Poiseuille flow with asymmetric convective cooling, Computers and Mathematics with Applications, 60(2010), 3012–3019, 2010.

[7] E. Fatunmbi and A. Adeniyan, Nonlinear Thermal Radiation and Entropy Generation on Steady Flow of Magneto-Micropolar Fluid Passing a Stretchable Sheet with Variable Properties, Results in Engineering, 6, 100142, 2020.

[8] B. Jha and M. Musa, The combined effects of anisotropic porous medium and stably stratified fluid on free convective flow through an annulus, Journal of Taibah University for Science. 12, 1-9, 2018

[9] J. A. Adigun, A. Adeniyan and I. O. Abiala, Stagnation point MHD slip-flow of viscoelastic nanomaterial over a stretched inclined cylindrical surface in a porous medium with dual stratification, International Communications in Heat and Mass Transfer, 126(2021), 105479.

[10] O. D. Makinde and A. S. Eegunjobi, Entropy Generation in a Couple Stress Fluid Flow Through a Vertical Channel Filled with Saturated Porous Media, Entropy 15(11), 4589-4606, 2013, https://doi.org/10.3390/e15114589.

[11] S. Baag, M. R. Acharya and G. C. Dash, MHD flow of a visco-elastic fluid through a porous medium between infinite parallel plates with time dependent suction, J Hydrodyn 27, 738–747, 2015, https://doi.org/10.1016/S1001-6058(15)60536-4.

[12] N. Z. Shehzad, A. Zeeshan, R. Ellahi and K. Vafai, Convective heat transfer of nanofluid in a wavy channel: Buongiorno's mathematical model, Journal of Molecular Liquids, 222, 446-455, 2016.

[13] A. Adeniyan and I. A. Abioye, Mixed convection radiating flow and heat transfer in a vertical channel partially filled with a Darcy-Forchheimer porous substrate, General Mathematics Notes, 32(2), 80, 2016.

[14] H. A. Isede and A. Adeniyan, Mixed convection flow and heat transfer of chemically reactive drilling liquids with clay nanoparticles subject to radiation absorption. Ain Shams Engineering Journal, 12(4), 4167-4180, 2021, https://doi.org/10.1016/j.asej.2021.04.030.

[15] A. Barletta, and E. Zanchini, Mixed convection with viscous dissipation in an inclined channel with prescribed wall temperatures, International Journal of Heat and Mass Transfer, 44, 4267-4275, 2001, 10.1016/S0017-9310(01)00071-0.

[16] M. M. Nganbe II, J. Hona, E. N. Nyobe and E. Pemha, Heat transfer and liquid distribution between two moving porous surfaces, J. Applied Sci., 17, 315-323, 2017.

[17] S. S. Okoya, Computational study of thermal influence in axial annular flow of a reactive third grade fluid with non-linear viscosity, Alexandria Engineering Journal, 58(1), 401-411, 2019.

[18] P. A. Davidson, An Introduction to Magnetohydrodynamics, Cambridge University Press, UK, 2002.

[19] J. Hartmann and F. Lazarus, Kongelige danske videnskabernes selskab, Matematisk-Fysiske Meddelelser, 15, 6-7, 1937.

[20] T. R. DePuy, Fluid dynamics and heat transfer in a Hartmann flow, MSc dissertation, Rensselaer Polytechnic Institute Hartford, Connecticut, USA, 2010.

[21] W. Jamshed et al., Evaluating the unsteady Casson nanofluid over a stretching sheet with solar thermal radiation: an optimal case study, Case Stud. Thermal Eng., 26, 101160, 2021.

[22] J. C. Umavathi and M. S. Malashetty, Magnetohydrodynamic mixed convection in a vertical channel, International Journal of Non-Linear Mechanics, 40, 91–101, 2005.

[23] M. G. Sobamowo, A. A. Yinusa and S. T. Aladenusi, Impacts of magnetic field and thermal radiation on squeezing flow and heat transfer of third grade nanofluid between two disks embedded in a porous medium, Heliyon, 6(2020), e03621, 2020.

[24] R. A. Damseh, T. A. Al-Azab, B. A. Shannak and M. Al Husein, Unsteady Natural Convection Heat Transfer of Micropolar Fluid over a Vertical Surface with Constant Heat Flux, Turkish J. Eng. Env. Sci., 31(2007), 225 – 233, 2007.

[25] S. Selimli and Z. Recebli, Impact of electrical and magnetic field on cooling process of liquid metal duct magnetohydrodynamic flow, Thermal Science, 22(1), 263–271, 2018, https://doi.org/10.2298/TSCI151110147S.

[26] A. Adeniyan, S.O. Kehinde, and G.M. Sobamowo, Impacts of slips on peristatic flow and heat transfer of micropolar fluids in an asymmetric channel, Mathematics in Engineering, Science and Aerospace (MESA), 13(4), 867-908, 2022.

[27] G. Degan, and P. Vasseur, Aiding Mixed Convection Through a Vertical Anisotropic Porous Channel With Oblique Principal Axes, International Journal of Engineering Science, 40, 193-209, 2002, 10.1016/S0020-7225(01)00012-X.

[28] S.J. Aroloye, O.J. Fenuga, A. Adeniyan. Surface radiation and mass flux effects on hydromagnetic anisotropic boundary-layer flow past a vertical plate with Ohmic and viscous dissipation. Journal of Scientific Research and Development (JSRD), 19(2) 13-29 http://jsrd.unilag.edu.ng/index.php/jsrd

[29] . Saouli and S. Aïboud-Saouli, Second-law analysis of laminar nonnewtonian gravity-driven liquid film along an inclined heated plate with viscous dissipation effect, Brazilian Journal of Chemical Engineering, 26, 2009, 10.1590/S0104-66322009000200019.

[30] K. Dwivedi, Adhesive wear behaviour of cast aluminium–silicon alloys: Overview, Materials & Design (1980-2015), 31(5), 2517-2531, 2010.

[31] S. Das and R. N. Jana, Entropy generation due to MHD flow in a porous channel with Navier slip, Ain Shams Engineering Journal, 5(2), 575-584, 2014, https://doi.org/10.1016/j.asej.2013.11.005

[32] O. D. Makinde, E. Osalusi, Second law analysis of laminar flow in a channel filled with saturated porous media, Entropy, 7(2), 148-160, 2005.

[33] S. Marzougui, M. Bouabid, M. Mebarek-Oudina, N. H. Abu-Hamdeh, M. Magherbi and K. Ramesh, A computational analysis of heat transport irreversibility phenomenon in a magnetized porous channel, International Journal of Numerical Methods for Heat & Fluid Flow, 33, 0961-5539, 2020, 10.1108/hff-07-2020-0418.

[34] H. Sato, The Hall Effects in the Viscous Flow of Ionized Gas between Parallel Plates under Transverse Magnetic Field, Journal of the Physical Society of Japan, 16, 1427-1433, 1961, http://dx.doi.org/10.1143/JPSJ.16.1427.

[35] M. Veera Krishna, and A. J. Chamkha, Hall Effects on Unsteady MHD Flow of Second Grade Fluid through Porous Medium with Ramped Wall Temperature and Ramped Surface Concentration, Phys. Fluids, 30, 053101, 2018, 10.1063/1.5025542.

[36] H. A. Isede., A. Adeniyan, Dissipative Nanofluid Slip-Flow and Heat Transfer in a Permeable Stretching Vertical Channel with Internal Heat Generation, International Journal of Mathematical Sciences and Optimization: Theory and Applications, 2020(1), 669-688.

[37] A. Adeniyan, G. M. Sobamowo., S. O. Kehinde, Impacts of Slips on Peristaltic Flow and Heat Transfer of Micropolar Fluids in an Asymmetric Channel, International Journal of Mathematical Sciences and Optimization: Theory and Applications (IJMAO), 7(2), 107-128, 2022. https://doi.org/10.5296.

[38] Bhatti, M. M., Eid, A., Khader, M. M. and Megahed, Ahmed M., Vieta-Lucas Collocation Technique for Examination of the Flow of Casson Fluid over a Slippery Stretching Sheet Which Is Impacted by Thermal Slip, Ohmic Dissipation, and Variable Thermal Conductivity, Journal of Mathematics (2033) 8723343. https:// doi.org/10.1155/2023/8723343